JOURNAL OF INFORMATION AND COMMUNICATION TECHNOLOGY
https://e-journal.uum.edu.my/index.php/jict

How to cite this article:
Aliyu, M. G., Jamel, S., & Danlami, M. (2026). An enhanced iris recognition using deep learning and 2D Chebyshev wavelet filter. *Journal of Information and Communication Technology, 25*(3), 98-123. https://doi.org/10.32890/jict2026.25.3.5

An Enhanced Iris Recognition using Deep Learning and 2D Chebyshev Wavelet Filter

[1]Muhammad Ghali Aliyu, [2]Sapiee Jamel & [3]Muktar Danlami
[1&2]Faculty of Computer Science and Information Technology, Universiti Tun Hussein Onn Malaysia, Malaysia
[3]Faculty of Computer Science and Information Technology, Northwest University, Nigeria

[*1]hi220014@student.uthm.edu.my
[2]sapiee@uthm.edu.my
[3]muktar@nwu.edu.ng
*Corresponding author

Received: 11/3/2026 Revised: 9/6/2026 Accepted: 9/6/2026 Published: 31/7/2026

ABSTRACT

Iris recognition is widely regarded as a reliable biometric authentication technique; however, its performance is often degraded by poor image quality, noise, eyelid and eyelash occlusion, illumination variation, off-angle acquisition, and partial iris visibility in unconstrained environments. This study proposes an enhanced iris recognition framework that integrates a Two-Dimensional Chebyshev Wavelet Filter (2DCWF) with a Convolutional Neural Network (CNN) to improve feature extraction, classification accuracy, and robustness under challenging imaging conditions. The proposed methodology consists of image acquisition from benchmark iris datasets, preprocessing through greyscale conversion, median filtering, and histogram equalisation, followed by iris segmentation using the Circular Hough Transform and normalisation using the Daugman rubber sheet model. The normalised iris images are then processed using the 2DCWF to extract discriminative multi-resolution spatial-frequency and texture features, which are supplied to a CNN classifier for identity recognition. The framework was evaluated using CASIA-IrisV4, UBIRIS.v2, and MMU datasets representing both controlled and unconstrained acquisition conditions. Experimental results show that the proposed 2DCWF-CNN model outperforms conventional feature extraction methods, including Gabor Wavelet Filter, Local Binary Pattern, and Legendre Wavelet Filter, achieving a highest recognition accuracy of 98.97%, with reduced False Acceptance Rate and False Rejection Rate and improved Genuine Acceptance Rate. These findings demonstrate that combining Chebyshev wavelet-based feature extraction with deep learning provides a robust and effective solution for reliable iris recognition in real-world biometric authentication systems.

Keywords: Biometric authentication, deep learning, 2D Chebyshev wavelet, feature extraction, iris recognition.

INTRODUCTION

In the realm of biometric authentication, iris recognition has emerged as a highly reliable method due to the unique and stable patterns of the human iris (Almolhis, 2024; Bonyani et al., 2022). Biometric systems have become integral to modern security and identification frameworks, leveraging unique physiological traits to authenticate individuals. Among these, iris recognition stands out due to its complex and distinctive patterns, which remain stable over a person's lifetime (Şerifi & Şerifi, 2025; Divya & Rajendra, 2022; Daugman, 2004). This stability and uniqueness make iris recognition a highly reliable method for personal identification. The complex patterns of the human iris remain stable throughout an individual's lifetime, rendering them highly suitable for accurate identification and verification (Hussein et al., 2026). Consequently, iris recognition systems have been widely adopted in various security applications, including border control, access management, and personal device authentication (Farouk et al., 2022; Huo et al., 2019).

A typical iris recognition system operates through four primary stages: "data acquisition, preprocessing, feature extraction, and matching or recognition" (Jagadeesh & Patil, 2018). Therefore, the system is heavily dependent on the quality of the captured iris images (Jalal & Ghanim, 2022). However, acquiring high-quality images is often challenging, especially in uncontrolled environments (Jamaludin et al., 2021). Factors such as motion blur, occlusions from eyelids and eyelashes, reflections from eyeglasses, and off-angle captures can degrade image quality, leading to increased false rejection rates and compromised system performance (Kumawat & Panda, 2023; Jan et al., 2020). Addressing these challenges necessitates robust feature extraction techniques capable of effectively handling such variabilities (Malgheet et al., 2021; Nithya & Lakshmi, 2019).

Feature extraction represents a crucial phase in the development of effective iris recognition systems, as it directly influences the system's ability to distinguish between individual iris patterns (Zambrano et al., 2022; Chen et al., 2020). Over the years, researchers have introduced various techniques to improve feature representation. Notable among these is the two-dimensional (2D) Gabor wavelet transform (Huo et al., 2019), Gabor filters (Sun et al., 2022), Scale-Invariant Feature Transform (SIFT) (Rathgeb et al., 2019), and Local Binary Patterns (LBP) (Taha & Ahmed, 2021). Among these, wavelet transform-based based have gained widespread popularity due to their effectiveness in mitigating some of these challenges by analyzing iris patterns at multiple scales and resolutions (Danlami et al., 2020; Rhif et al., 2019; Fathi & Mohamadi, 2019). The wavelet transform decomposes images into multiple frequency components, facilitating efficient coding and compression while preserving critical image features necessary for accurate recognition. This multi-resolution analysis allows for effective feature extraction, capturing both global and local iris characteristics (Mukherjee et al., 2021). However, the iris features are frequently distorted, noisy, or obstructed, making feature extraction and matching difficult. Furthermore, authentication of noisy (Occluded by eyelash or eyelid), angular images, and incomplete or partially captured images is challenging and needs improvement (Dahan & Jaha, 2025). To tackle this problem, this study proposed a novel 2D-Chebyshev wavelet filter (2DCWF), a type of wavelet transform that uses Chebyshev polynomials of different kinds to construct wavelet basis functions. It has compact support, which leads to efficient computation, sparse representation, orthogonality, high resolution, functional approximation, and rotation invariance, which make it suitable for feature extraction. Integrating deep learning methodologies with wavelet-based signal processing presents a robust and effective framework for enhancing the performance of iris recognition systems. This study introduces a novel deep learning framework that synergistically combines 2DCWF with a Convolutional Neural Network (CNN), aiming to enhance the extraction of salient iris features for iris recognition. The system demonstrates improvements in recognition accuracy, robustness to noise, and computational efficiency. It also advances the field of iris recognition, offering a robust solution capable of operating effectively in challenging real-world scenarios. The remainder of this article is: Related Literature, Methodology, Experiments, and Conclusion.

RELATED WORKS

The standard pipeline for iris recognition includes segmentation, localization, normalization, feature extraction, and matching (Toizumi et al., 2023). Among these stages, image quality degradation has a pronounced impact, particularly on feature extraction. Segmentation and localization methods typically utilize global edge features, such as those defining the iris and pupil boundaries (Zhao et al., 2021). However, feature extraction relies heavily on the availability of detailed texture information from both local and global regions of iris. Noise images often fail to preserve fine-grained texture details, resulting in diminished feature quality compared to images captured under a controlled environment. To address this, several recent studies have proposed resolution-robust feature extraction techniques that maintain recognition performance under varying image quality (Boutros et al., 2022; Guo et al., 2019).

Traditional iris recognition systems employ hand-crafted feature descriptors to encode normalized iris images into fixed-length templates. Techniques such as Gabor filters and phase-based representations have been widely used (Sun et al., 2022; Czajka et al., 2019; Miyazawa et al., 2008; Daugman, 2004). These descriptors are then compared using distance metrics such as HD to facilitate matching. While effective in controlled settings, these methods typically struggle in unconstrained environments with noisy or occluded data. To overcome these limitations, recent research has increasingly turned to deep learning-based solutions, which have shown promise in enhancing recognition accuracy and robustness under degraded image conditions (Jalilian et al., 2022; Kawakami et al., 2022; Wei et al., 2022). Many of these approaches utilize metric learning frameworks, which train neural networks to learn similarity-preserving embeddings. This enables the recognition of unknown classes and supports generalization beyond the training dataset.

Banerjee et al. (2022) introduced a V-Net-based architecture for iris segmentation in challenging environments. This model synthesizes semantic segmentation masks and employs a color-space segmentation technique to refine iris boundaries. Achieving a mean Intersection-over-Union (IoU) of 95.6% on the UBIRIS dataset, the V-Net architecture significantly outperformed the traditional U-Net model. Nsaif et al. (2022) proposed an iris recognition approach that uses a combination of Multi-Scale Grey-Level Co-occurrence Matrix (MSGLCM) and Multi-Range Circle Hough Transform (MRRCHT) for accurate segmentation in dynamic imaging environments. Tested on the “CASIA.v4.0 (Distance) and MMU.v2 databases”, the model achieved high recognition accuracy and reduced processing time.

Meanwhile, Virtusio et al. (2022) implemented a practical iris recognition system using multi-level Otsu thresholding and the Daugman algorithm on a Raspberry Pi platform. This lightweight solution improved recognition accuracy from 94.23% to 96.60% through enhanced preprocessing, highlighting the potential of low-cost systems in real-world biometric applications. Regencia et al. (2023) explore the integration of fuzzy logic into the iris recognition system and an enhanced Morlet wavelet transform for feature extraction. The image is pre-processed using Gaussian Blur and Canny Edge detection. The Morlet Wavelet is combined with a fuzzy logic model to enhance the features extracted from the iris image, supporting the making of accurate decisions. The fuzzy logic model is then used to classify the input features. The 700 image datasets are generated by the researchers, and they contain some noise, such as blurred images, off-angle, and occlusion. The approach indicated that 85.43% overall accuracy was achieved. However, the system works on non-ideal datasets with poor recognition accuracy, and an additional technique is required to improve the system’s performance.

Nguyen et al. (2023) proposes a complex-valued neural network for iris recognition, improving upon traditional real-valued models by capturing both phase and magnitude information from iris textures. It is evaluated using the ND- CASIA.Iris-Thousand, CrossSensor-2013, and UBIRIS.v2 datasets, exhibiting superior performance characterized by EER and enhanced feature discriminability compared to existing real-valued deep learning approaches. However, the increased computational cost of training a fully complex-valued network poses a challenge for real-time deployment. In addition, its robustness against degraded or occluded iris images requires further investigation. A 2D Gabor filter for improving iris recognition accuracy by capturing both local and global texture details from iris images is proposed (Ibrahim & Sultan, 2023). The 2D Gabor filter is applied to extract iris features by analyzing frequency components in multiple orientations and optimized using Artificial Bee Colony (ABC) to improve classification. The ABC algorithm clusters iris data, reducing computational overhead and improving accuracy to optimize feature selection. Their approach is tested using 280 iris images acquired from 28 subjects and achieved good recognition accuracy. However, the dataset used is small, which may constrain the generalizability of the results to be broader. In addition, the real-time efficiency of the approach is not extensively analyzed, raising concerns about its practical deployment in high-speed security applications.

Furthermore, Rathnayake et al. (2023) proposed a real-time iris extraction system adaptable to various imaging conditions using CNN. It focuses on improving iris extraction for both near-infrared (NIR) and visible spectrum (VS) images while addressing challenges such as illumination variations, occlusions, and low-quality imaging. A U-Net architecture with a pre-trained ResNet34 backbone is used, and the model also applies a modified CHT for precise iris segmentation and boundary detection. Performance is evaluated using diverse datasets, with pixel error as the primary metric and real-time processing validated through execution time. However, it has limitations, including errors in challenging conditions, a lack of diversity in the dataset, and a real-time execution speed (10 FPS) that may be insufficient for ultra-fast security applications. Despite these challenges, the study advances iris recognition technology by improving CNN-based segmentation techniques, indicating the potential of deep learning-driven biometric solutions while emphasizing areas for further improvement.

In addition, a study aims to improve iris recognition accuracy by developing the ‘EnhanceDeepIris’ model, which integrates deep convolutional features with sequential metric modelling (He & Li, 2024). Its primary objectives include enhancing feature extraction, addressing iris texture deformation, and improving model robustness across diverse datasets. The methodology involves leveraging deep CNNs for feature extraction and incorporating a sequential metric model to handle radial iris texture distortions. The model achieves a high accuracy of 99.88%, while improving robustness against noise and occlusions. However, the model struggles with severely degraded or occluded iris images, affecting its performance in challenging real-world scenarios. Furthermore, while tested on standard datasets, its generalizability is uncertain due to a lack of evaluation on more diverse real-world datasets.

Chen et al. (2024) aims to address the persistent challenge of recognising and processing irregularly incomplete iris images. To achieve this, the authors propose a Two-Stage and Two-Discriminator Generative Adversarial Network (TT-GAN). These perform coarse-to-fine iris image inpainting using gated convolution and a Pixel–Channel (PC) attention mechanism, while enforcing both global and local consistency through dual SN-PatchGAN discriminators. Experiments were conducted on “IITD, CASIA-Iris-Interval, and UBIRIS.V2 databases”. The results demonstrate substantial improvements in both image quality and recognition performance after restoration, with PSNR increases of up to 24.61 dB, SSIM improvements up to 0.13. The recognition accuracy is improved by 93.42% (IITD), 68.41% (CASIA-Iris-Interval), and 59.72% (UBIRIS.V2) compared to incomplete images. Despite its strong performance, the study is limited by its reliance on explicit mask annotations to indicate missing regions, which can be time-consuming for large-scale deployment, and by reduced restoration fidelity when dealing with very large missing areas and complex iris textures, indicating room for further improvement in fully automated and highly degraded scenarios.

Sharma et al. (2025) proposed an enhanced iris recognition framework based on Histogram Cut Selection and Genetic Algorithms. The objective was to improve iris feature extraction, segmentation, and classification accuracy under varying illumination and occlusion conditions. A histogram Cut Selection was used for feature extraction and segmentation, recursive entropy discretization for improved segmentation precision, and a Genetic Algorithm-optimized classifier to refine decision boundaries. The model was evaluated on CASIA-IrisV4 and IITD datasets, and the proposed approach achieved 98.7% training accuracy, 97.8% testing accuracy, and 97.7% validation accuracy, outperforming several methods such as MLRP-GDF, MCSVM, CNN-ANFIS, VGG16-SVM, CNN-LSTM, and SDD-CNN. However, the approach relies on GA-based optimisation, which may increase computational complexity and may not generalize as efficiently as CNN-based hierarchical learning when applied to larger or noisier datasets.

Louriga et al. (2026) introduced a hybrid multi-domain feature fusion model integrating Multivariate Ensemble Empirical Mode Decomposition, VGG16, ResNet-152, and Local Binary Patterns. The objective was to improve iris recognition by combining statistical, global, and local texture representations into a compact discriminative feature vector. They used MEEMD to capture nonlinear and nonstationary iris variations, then extracted deep semantic features using pretrained VGG16 and ResNet-152, while LBP was used for local micro-texture encoding. PCA was applied for dimensionality reduction, and classification was performed using multiple machine learning classifiers with hyperparameter tuning. The model achieved up to 98% on IITD, 97% on CASIA, and 97.30% on UBIRIS.v2. However, the framework is relatively complex, involving multiple feature sources and dimensionality reduction steps, which may increase computational cost and reduce architectural simplicity.

Rahman et al. (2025) investigated distant iris recognition using deep feature transfer and machine learning classifiers. The objective was to address recognition challenges caused by distance-based acquisition, small iris regions, illumination variation, and class imbalance. The study extracted features from normalized iris images using a customized 32-layer CNN as well as pretrained VGG16, VGG19, and ResNet50 models. These extracted deep features were then classified using nine machine learning algorithms, including RF, LDA, KNN, SVM, Naïve Bayes, Decision Tree, MLP, Extra Trees, and Softmax. The best result was obtained using the customized CNN with Softmax, achieving 93.40% accuracy, 94.31% precision, 93.40% recall, 93.25% F1-score, and 93.34% Cohen’s kappa on CASIA-V4. However, the model is its sensitivity to class imbalance, possible overfitting, and dependence on normalized images.

Recent studies further confirm that robust iris recognition under degraded and unconstrained imaging conditions remains an unresolved research problem. Nguyen et al. (2024) reviewed recent deep learning-based iris recognition methods and showed that, despite significant progress, robustness across segmentation, recognition, and practical deployment scenarios remains a major research concern. Similarly, AlRifaee et al. (2024) demonstrated that when conventional cooperative acquisition conditions are relaxed, iris recognition performance deteriorates due to segmentation and feature extraction errors in unconstrained environments. Shoji et al. (2024) further emphasised that less-constrained acquisition often introduces low resolution, optical down-sampling, and out-of-focus blur, which reduce the visibility of discriminative iris texture and directly affect feature extraction. Recent deep learning models have attempted to address these limitations through multiscale attention, adaptive segmentation, and improved feature learning; however, such approaches may still involve increased computational complexity or insufficient preservation of localised spatial-frequency iris texture (Luo et al., 2025; Guo et al., 2025). Farmanullah (2026) demonstrated that robust segmentation remains critical in non-ideal iris systems, particularly when images contain closed eyes, occlusions, reflections, blur, and non-uniform illumination. Similarly, Sharma et al. (2025) showed that optimised feature selection and evolutionary classification can improve recognition accuracy, while Louriga et al. (2026) further confirmed the effectiveness of integrating signal-processing descriptors with CNN-derived representations. Therefore, there remains a clear need for a computationally efficient feature extraction framework capable of capturing discriminative multi-resolution iris texture while improving robustness to noise, occlusion, illumination variation, and partial iris visibility. This gap motivates the proposed integration of a Two-Dimensional Chebyshev Wavelet Filter (2DCWF) with a CNN classifier.

METHODOLOGY

This section presents the methodological framework developed for robust iris recognition under degraded and unconstrained imaging conditions. The proposed approach is designed to address the major limitations identified in the literature, including noise, eyelid and eyelash occlusion, illumination variation, off-angle acquisition, partial iris visibility, and reduced texture quality. To achieve this objective, the framework integrates image enhancement, circular iris localisation, polar normalisation, 2DCWF-based feature extraction, and CNN-based classification. The rationale for this integration is that preprocessing improves image quality, segmentation isolates the valid iris region, normalisation compensates for geometric variation, 2DCWF extracts discriminative multi-resolution spatial-frequency texture features, and CNN classification learns hierarchical representations from the extracted feature maps. The complete workflow of the proposed method is shown in Figure 1 and the details explanation of the processes is provided in subsection below.

Iris Image Acquisition

In the first stage, iris images were obtained from benchmark datasets, including CASIA-IrisV4, UBIRIS.V2, and MMU.V2. These datasets were selected because they represent both controlled and unconstrained acquisition conditions, thereby allowing the robustness of the proposed method to be evaluated under variations in illumination, occlusion, off-angle capture, image resolution, and partial iris visibility. The CASIA- IrisV4 consists of iris images captured in controlled environments, using near-infrared (NIR) imaging. This ensures high contrast between the iris and pupils, making it suitable for precise feature extraction and segmentation. In contrast, the UBIRIS-V2 database includes noisy and visible spectrum (VS) images obtained in uncontrolled settings, introducing real-world challenges such as lighting variations, occlusions, and reflections. These conditions make UBIRIS-V2 an ideal dataset for evaluating the system’s performance under challenging imaging scenarios. Meanwhile, the MMU.V2 database contains iris images captured under varied lighting conditions and subject movements, simulating real-life fluctuations in image quality and positioning. Figure 2 shows captured iris images with different levels of noise.

Figure 1

Proposed 2DCWF- CNN Framework for Iris Recognition

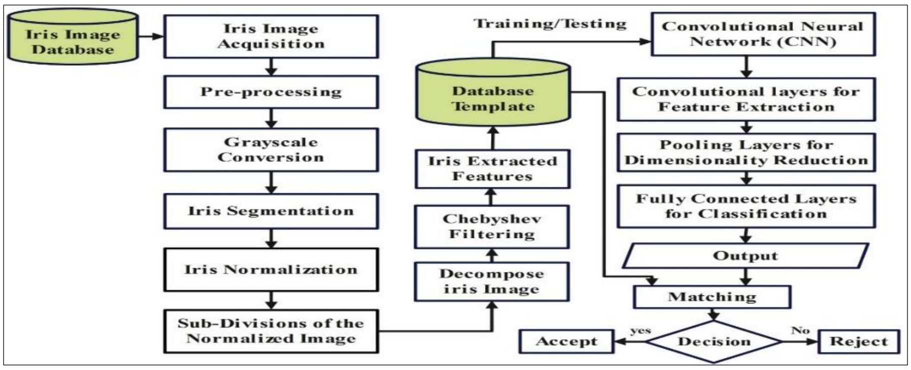

Figure 2

An Example of Iris Images with Occlusions from UBIRIS and MMU Datasets: A & B (Off-Angle), C & D (Incomplete Captured Iris Image), E & F (Eye-Glasses), and G & H (Occlusions by Eyelashes)

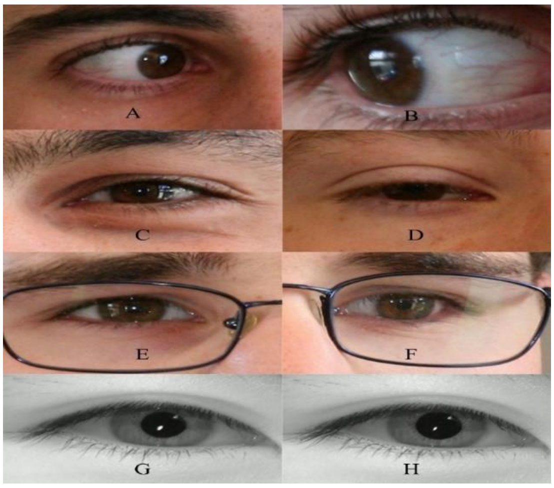

Pre-processing

Preprocessing reduces sensor noise, improves contrast, and stabilizes texture visibility before segmentation and feature extraction. Median filtering of the converted RGB to grayscale image was applied to suppress impulsive noise while preserving edge information, which is essential for accurate iris boundary localisation. Histogram equalisation was then used to enhance local contrast and improve the visibility of fine iris texture patterns as expressed in Equation (1-3).

$$I_{Gray} = 0.2989 \times R + 0.5870 \times G + 0.1140 \times B \tag{1}$$

where, R, G, B characterize as the intensity values of the red, green, and blue channels, respectively, and I_{Gray} represents the corresponding grayscale intensity value for each pixel.

$$I_{Filtered} = Median\left\{I_{Gray}\,(m, n)\right\} \tag{2}$$

where, $I_{Filtered}$ (i, j) is the noise-free pixel value, and I_{Gray} (m,n) represents the grayscale intensity values in the local window.

$$I_{HE}(x,y) = \left(\frac{CDF(I_{Filtered}\,(x,y)) - CDF_{min}}{(M \times N) - (CDF_{min})}\right) \times 255 \tag{3}$$

where, $I_{HE}(x,y)$ serve as the new intensity value at pixel *(x,y)* and $CDF(I_{Filtered}(x,y))$ represents the cumulative distribution function (CDF) of the image. CDF_{min} is the minimum value of *CDF* (avoid division by zero). While $(M \times N)$ is the total number of pixels in the image. The *CDF* redistributes pixel intensities to spread them out more evenly across the available range (0-255).

Segmentation

Iris images may contain occlusions (eyelashes, eyelids, or reflections) and variations in pupil dilation; precise localization is necessary to obtain a consistent iris representation (Farmanullah, 2026).

$$(x - x_0)^2 + (y - y_0)^2 = r^2 \tag{4}$$

where, x_0, y_0 represents the Centre coordinates of the circle, and the points along the circle's boundary are *(x, y)*

The iris structure is categorized by two concentric circular edges: the outer boundary delineating the iris from the surrounding sclera and the inner boundary separating the pupil from the iris. This study employed CHT to detect the iris boundaries accurately, as described in Equation 5.

$$H(x_0, y_0, r) = \sum_{x,y} \delta[(x - x_0)^2 + (y - y_0)^2 - r^2] \tag{5}$$

where, δ is an indicator function that accumulates edge points contributing to a possible iris boundary. The high value in Hough space corresponds to the best-fitting circle, which is then used to localize the iris region.

To handle partial this framework employs a robust segmentation approach that dynamically processes iris images based on the available occluded region to ensure reliable recognition. In the conventional systems, heavily occluded images are discarded, but this framework allows the system to handle iris images with as little as 12.5% of the iris region, ensuring adaptability in challenging environments.

The segmentation thresholds are as follows:

$$P_{valid} = \left(\frac{A_{valid}}{A_{total}}\right) \times 100\% \tag{6}$$

The threshold values (ρ_{valid}) of partial iris recognition is handled as far the following conditions:

P =100%, full iris available (100%), standard Chebyshev feature extraction is applied.
P ≥ 75% (Minimal Occlusion), minor occlusions are detected using edge-based segmentation and masked before feature extraction. Then, the standard Chebyshev feature extraction is applied.
P ≥ 50% to *P ≤74.9%* (Moderate Occlusion), morphological operators and local contrast enhancement compensate for missing regions, before standard Chebyshev feature extraction is applied.

$P \geq 25\%$ to $P \leq 49.9\%$ (Severe Occlusion), the system applied a sector-based feature extraction using Chebyshev feature extraction, where only the most information-rich segments of the iris contribute to recognition.
$\rho \geq 16.5\%$ to $\rho \leq 24.9\%$: the minimal portion of the iris image will be used to extract features using chebyshev filter. The extracted feature from each piece is matched with the iris image saved in the database.
$\rho \geq 12.5\%$ to $\rho \leq 24.9\%$ (Extreme Occlusion), region-based normalisation is used before Chebyshev feature extraction is applied to extract as much information as possible.

Normalisation

Normalisation transforms the circular iris into a fixed-dimension representation, making it consistent across different images and individuals. The process starts after the iris image is localized to account for pupil dilation, off-angle variations, and varying iris sizes. This is achieved by applying the "Daugman Rubber Sheet Model to convert the iris from Cartesian coordinates (x, y) to polar coordinates (r, θ)", and it is depicted in Figures 3 and 4 using two different databases.

$$I(x,y) \rightarrow I(r,\theta) \tag{7}$$

where r is equivalent to radial distance from the pupil boundary to the sclera, and θ is the angle of polar coordinates.

Figure 3

Detected Iris/Pupil and Normalization using MMU Database

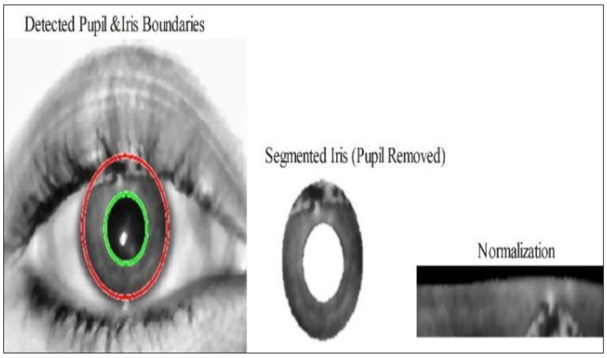

Figure 4

Detected Iris/Pupil and Normalisation using CASIA.v4 Database

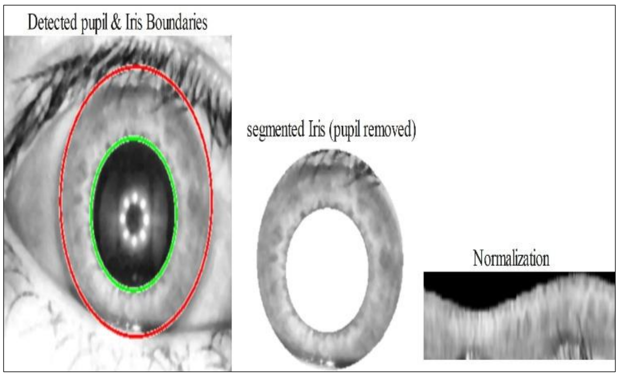

Feature Extraction

This process converts the raw iris texture into numerical representations that can be used for classification. The effectiveness of a recognition system largely depends on the choice of feature extraction method, as it determines how well the system can distinguish between different individuals. Feature extraction was performed using the proposed Two-Dimensional Chebyshev Wavelet Filter. The 2DCWF decomposes the normalised iris texture into multi-resolution spatial-frequency components using Chebyshev polynomial basis functions. This allows the method to capture both localised texture variations and frequency-domain characteristics of the iris. Compared with conventional descriptors, the 2DCWF provides compact support, orthogonality, sparse representation, and improved localisation of discriminative iris texture.

The construction of the Chebyshev wavelet was derived from a recursive Chebyshev polynomial and achieved using multi-resolution analysis (Guariglia & Guido, 2022). Chebyshev polynomials $T_m(x)$ are orthogonal polynomials on the interval [-1,1] defined recursively. Orthogonality ensures that the features are extracted independently to get a comprehensive image representation. $T_0(x) = 1$, $T_1(x) = x$,

$$T_{m+1}(x) = 2xT_m(x) - T_{m-1}(x) \tag{8}$$

One-dimensional Chebyshev wavelet:

$$\Psi_{n,m}^{k}(x) = \begin{cases} \eta_m \, \mu^{\frac{k}{2}} \, T_m\left(2\mu^k x - 2n + 1\right), & \frac{n-1}{\mu^k} \le x < \frac{n}{\mu^k} \\ 0, & otherwise \end{cases} \tag{9}$$

where, $\Psi_{n,m}^{k}(x)$ is the Chebyshev wavelet function indexed by scale k, position n and order m. η_m represents normalisation factor, while μ is an integer that controls scale and resolution in the contractive mapping.

Two-dimensional Chebyshev wavelet:

$$\Psi_{n_1,m_1,n_2,m_2}^{k}(x,y) = \Psi\,(k_1 n_1 m_1, x)\,\Psi\,(k_2 n_2 m_2, y) \tag{10}$$

$$\Psi_{n_1,m_1,n_2,m_2}^{k}(x,y) = \begin{cases} \eta_{m_1}\eta_{m_2}\mu^{\frac{k_1+k_2}{2}} \, T_{m_1}(2\mu^{k_1}x - 2n_1 + 1) \times T_{m_2}(2\mu^{k_2}y - 2n_2 + 1) \\ \qquad \frac{n_1-1}{\mu^{k_1}} \le x < \frac{n_1}{\mu^{k_1}}, \frac{n_2-1}{\mu^{k_2}} \le y < \frac{n_2}{\mu^{k_2}} \\ 0, \qquad otherwise \end{cases} \tag{11}$$

where, $\Psi_{n_1,m_1,n_2,m_2}^{k}(x,y)$ Represents the two-dimensional wavelet function indexed by scaling parameters k_1, k_2, position indices n_1, n_2, and order m_1, m_2. While η_{m_1}, η_{m_2} are normalization factors and μ^{k_1}, μ^{k_2} represents positive integers that control the scale and resolution in the contractive mapping.

The Chebyshev polynomials are computed recursively to serve as wavelet basis functions as in line 2 of Algoritm 1. These polynomials are then used in wavelet decomposition, where the iris image is transformed using 2DCWF to generate approximation and detail coefficients as indicated in line 3. In line 4, a multi-level wavelet decomposition is performed, which partitions the image into four distinct sub-bands: LL (approximation), LH (horizontal detail), HL (vertical detail), and HH (diagonal detail) components. After decomposition, statistical features such as mean, variance, skewness, kurtosis, entropy, and wavelet moments are extracted to form a structured feature vector. These extracted features are then stored and formatted for classification.

Algorithm 1: Feature Extraction Using 2DCWF Integrated with CNN and Matching	
1.	Start
2.	Define Chebyshev polynomial function:
	Compute basis polynomials recursively:
	$T_0(x) = 1$
	$T_1(x) = x$
	$T_m(x) = 2x * T_{(m-1)}(x) - T_{(m-2)}(x)$
3.	Apply wavelet decomposition:
a.	Compute wavelet coefficients using:
	$\Psi^{k}_{n_1,m_1,n_2,m_2}(x,y) = \eta_{m_1}\eta_{m_2}\mu^{\frac{k_1+k_2}{2}} T_{m_1}\left(2\mu^{k_1}x - 2n_1 + 1\right) \times T_{m_2}\left(2\mu^{k_2}y - 2n_2 + 1\right) e^{i2\pi(u_1x+v_1y)}$
b.	Extract approximation and detail coefficients
4.	Perform multi-level wavelet decomposition:
	Extract LL, LH, HL, HH sub-bands
5.	Store the extracted feature set
6.	Define CNN architecture:
a.	Input layer → Accept feature matrix
b.	Convolutional layers → Extract spatial features using: $z^{(l)}_{i,j} = \sum_{n}\sum_{n} W^{(l)}_{m,n} X^{(l-1)}_{(i+m)(j+n)} + b^{l}$
c.	Apply ReLU activation: $A^{(l)}_{i,j} = \text{Max}\,(0, z^{(l)}_{i,j})$
d.	Pooling layers → Reduce feature dimensions: $P^{(l)}_{i,j} = \max(A^{(l)}_{2i,2j,}\ A^{(l)}_{2i,2j+1,} A^{(l)}_{2i+1,2j+1,})$
e.	Fully connected layers → Map features to classes: $O_k = f\left(\sum_{j} W^{(fc)}_{jk}\ P^{(l)}_{j} + b^{(fc)}_{k}\right)$
f.	Apply Softmax for final classification: $\hat{y}_k = \frac{e^{O_k}}{\sum_j e^{O_j}}$
7.	Train the CNN model using feature vectors and labels
8.	Predict iris class using trained CNN model
9.	Store predicted class label
10.	Proceed to matching and decision-making
11.	Compare extracted feature set with stored templates in the database
12.	Compute similarity measure (Hamming Distance): $HD = \frac{1}{N}\sum_{j=1}^{N} X_j \oplus Y_j$
13.	Compare with threshold (τ):
	If D_H ≤ τ → Match (Authentication Successful)
	Else → No Match (Authentication Failed)
14.	Store authentication decision
15.	End

Figure 5 presents the three-dimensional surface representation of the proposed 2DCWF generated at orders (n_x = 4) and (n_y = 5). The surface illustrates the oscillatory and localised behaviour of the Chebyshev wavelet basis across the spatial domain. The alternating positive and negative amplitudes represent the filter's ability to respond to variations in iris texture intensity, particularly fine structural changes caused by crypts, furrows, freckles, collarette patterns, and radial texture components. The colour scale indicates the magnitude of the wavelet response, with high positive and negative amplitudes corresponding to regions of strong local frequency variation. This property is important in iris recognition because discriminative iris information is often embedded in subtle spatial-frequency variations rather than in global intensity patterns alone. The surface pattern further demonstrates the multi-resolution capability of the 2DCWF. The smooth but repeated peaks and troughs show that the filter can decompose iris texture into localised frequency components while preserving spatial structure.

Figure 5

Three-dimensional Surface Representation of the 2D Chebyshev Wavelet Filter at Order n_x = 4, and n_y = 5

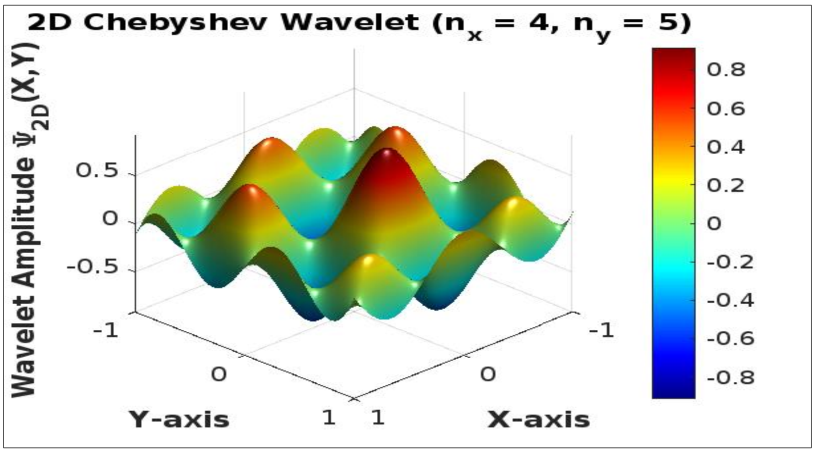

Figure 6 shows the contour representation of the 2DCWF at orders (n_x = 4) and (n_y = 5). Unlike the three-dimensional surface plot, the contour view provides a two-dimensional spatial interpretation of the wavelet response distribution. The alternating regions of high and low intensity show how the Chebyshev wavelet partitions the image plane into localised response zones. These zones are useful for detecting spatially varying iris texture patterns, especially in normalised iris images where discriminative features are distributed across radial and angular directions. The presence of both concentrated and smoothly varying response regions indicates that the filter can capture fine texture details as well as broader structural variations. The contour response is important because iris images acquired under unconstrained conditions often contain non-uniform illumination, partial occlusion, and local texture degradation. The localised response structure of the 2DCWF allows the feature extraction stage to emphasise informative regions while minimising the influence of degraded or less discriminative areas. Therefore, the contour representation supports the methodological justification for using 2DCWF as a feature extraction filter before CNN classification. It visually confirms that the proposed filter is capable of generating spatial-frequency representations suitable for robust iris recognition under both controlled and challenging acquisition conditions.

Figure 6

Contour Representation of 2DCWF at Order n_x = 4, and n_y = 5

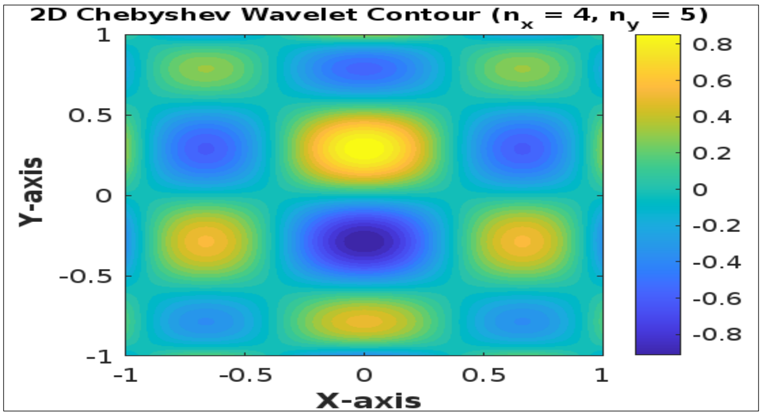

The extracted feature response obtained after applying the 2DCWF to the normalised iris image is presented in Figure 7. The horizontal axis represents the feature index, while the vertical axis shows the corresponding wavelet feature amplitude. The plot demonstrates that the 2DCWF produces a rich and highly variable feature representation, with both positive and negative coefficient responses distributed across the feature space. These variations indicate the presence of discriminative iris texture information captured from different spatial-frequency regions of the iris image. The negative and positive coefficient distributions reflect the filter's ability to encode contrast changes and directional texture variations within the iris.

Figure 7

Extracted Features using 2DCWF

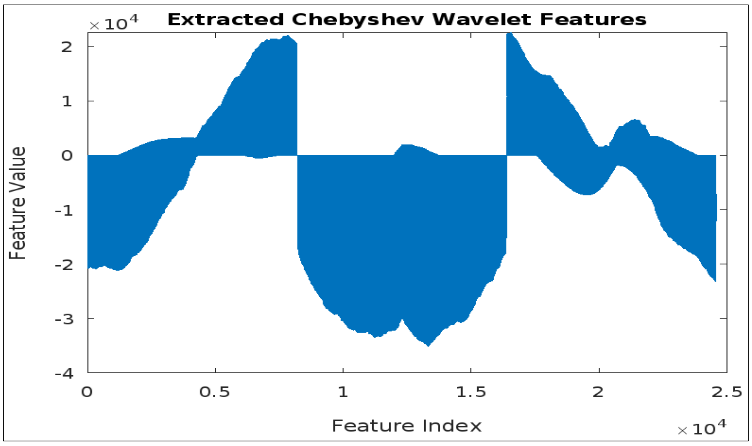

The implementation of the CNN-based iris classification using CWT features in MATLAB follows a structured process. The pre-extracted iris feature matrix is loaded, where features have been obtained using the 2DCWF to enhance texture details. The data is then normalized to ensure consistency in training, and class labels are converted into a categorical format to be compatible with MATLAB's deep learning framework. Then, the CNN architecture comprises an input layer followed by convolutional layers designed to extract spatial features from the iris images. Each convolutional layer is paired with batch normalization to improve training stability and ReLU activation functions to introduce non-linearity. Pooling layers are incorporated to perform down-sampling, reducing dimensionality and computational complexity. The extracted feature maps are then passed through fully connected layers, which map them to class-specific outputs a softmax activation function is applied to convert these outputs into probability distributions for multi-class classification as summarise in Table 1.

Table 1

CNN Architecture and Training Configuration for Reproducibility

Component	Specification
Feature input	2DCWF-extracted iris feature matrix
Class labels	Converted to categorical labels for CNN classification
Software environment	MATLAB Deep Learning Toolbox
Input layer	Feature input layer accepting the 2DCWF feature representation
Convolutional layers	Convolutional layers used for spatial feature learning from 2DCWF feature maps
Normalisation layer	Batch normalisation applied after convolutional operation
Activation function	Rectified Linear Unit (ReLU)
Pooling operation	Max-pooling for dimensionality reduction
Fully connected layer	Used to map learned feature representations to iris identity classes
Output layer	Softmax layer followed by classification layer
Optimiser	Adam optimiser
Initial/base learning rate	0.0010
Maximum epochs	50
Total recorded iterations	50
Mini-batch accuracy at Epoch 1, Iteration 1	20.00%
Mini-batch loss at Epoch 1, Iteration 1	6837.6533
Mini-batch accuracy at Epoch 50, Iteration 50	100.00%
Mini-batch loss at Epoch 50, Iteration 50	0.0000e+00
Training stopping condition	Maximum epochs completed
Training duration	Approximately 1 second
Data partitioning	70% training and 30% testing
Evaluation metrics	Accuracy, FAR, FRR, GAR, EER, and Hamming Distance-based matching decision
Baseline comparison	LBP, Gabor Wavelet Filter, and Legendre Wavelet Filter under the same "preprocessing, segmentation, normalisation, and evaluation protocol"

The CNN was trained using 2DCWF-extracted iris feature representations as input. Training was implemented in MATLAB using the Adam optimiser with an initial learning rate of 0.0010 and a maximum of 50 epochs. The training log showed an initial mini-batch accuracy of 20.00% with a loss value of 6837.6533 at Epoch 1, Iteration 1. At Epoch 50, Iteration 50, the mini-batch accuracy reached 100.00%, while the mini-batch loss decreased to 0.0000e+00, indicating convergence of the model on the training mini-batches. Training was terminated after the maximum number of epochs was completed. To ensure fair evaluation, the trained CNN was assessed using the reserved testing samples, and performance was measured using recognition accuracy, FAR, FRR, GAR, EER, and accuracy.

To further validate the contribution of each major component of the proposed framework, an ablation study was designed to examine the effect of the 2DCWF feature extraction module and the CNN classifier on iris recognition performance. The ablation analysis was conducted using the same datasets, preprocessing procedure, segmentation method, normalisation approach, data partitioning strategy, and evaluation metrics to ensure a fair comparison. Four experimental configurations were considered. First, a CNN-only model was evaluated using the normalised iris images without 2DCWF enhancement to determine the baseline learning capability of the classifier. Second, a 2DCWF-based model with Hamming Distance matching was tested to assess the standalone discriminative strength of the Chebyshev wavelet features. Third, conventional feature descriptors, including LBP, GWF, and LWF, were integrated with the CNN classifier to compare their performance with the proposed Chebyshev-based representation under identical classification conditions. Finally, the complete 2DCWF-CNN framework was evaluated to determine the combined effect of multi-resolution Chebyshev wavelet feature extraction and deep hierarchical classification. This ablation design allows the performance gain of the proposed method to be attributed more clearly to the 2DCWF module, the CNN classifier, and their integration, thereby strengthening the methodological robustness and reproducibility of the study.

Matching

In this phase, the extracted feature vector is matched against pre-stored templates within the system database to verify or establish identity. This matching procedure employs the HD, as indicated in line 12 of the algorithm. The HD serves as a similarity measure by quantifying the number of bit-wise discrepancies between the binary feature representation of the test image and those of the enrolled template.

EXPERIMENT

A series of experiments were conducted using widely recognized benchmark iris databases to assess the effectiveness of the proposed iris recognition framework based on the 2DCWF. These datasets comprise an iris image captured under different conditions such as occlusions, off-angle, and changes in illumination that enable a comprehensive evaluation of the system’s robustness. Each experiment was structured into enrolment, training, and testing phases to evaluate the framework’s performance rigorously. Table 2 shows the details of selected iris images and their corresponding subjects in each database. For each dataset, 70% of the images per subject were allocated for training, while the remaining 30%, consisting of occluded or partially visible iris samples, were reserved for testing to simulate real-world recognition challenges.

Table 2

Description of Selected Databases

S/no.	Databases	Subject	Images	Format
1	UBIRIS.v2	261	1,170	tiff
2	MMU.v2	46	450	bmp
3	CASIA.v4 Distance	142	1,320	jpg
4	CASIA.v4 Interval	249	1,250	jpg

The ablation analysis was conducted to examine the individual and combined contributions of the CNN classifier and the proposed 2DCWF feature extraction module. As shown in Table 3, the CNN-only configuration produced lower recognition performance across all datasets compared with the complete 2DCWF-CNN framework. This indicates that although CNN is capable of learning discriminative representations from iris images, its performance is reduced when the input features are not enhanced by a robust spatial-frequency descriptor. This reduction is more evident in unconstrained datasets such as UBIRIS.v2 and CASIA.v4-Distance, where noise, illumination variation, off-angle acquisition, and partial iris visibility degrade the quality of the raw iris texture. The 2DCWF with Hamming Distance configuration achieved better performance than the CNN-only model, demonstrating the standalone discriminative strength of the Chebyshev wavelet representation. This confirms that the 2DCWF is effective in extracting multi-resolution texture features from the iris by preserving localised spatial-frequency information. However, its performance remained lower than the complete 2DCWF-CNN framework, indicating that handcrafted similarity matching alone is less adaptive than deep hierarchical classification. The conventional descriptor-based CNN configurations, including LBP-CNN, GWF-CNN, and LWF-CNN, produced competitive but lower recognition accuracy than the proposed method. This suggests that although conventional descriptors can capture certain local or frequency-based iris features, they are less effective in representing degraded and partially visible iris patterns under unconstrained imaging conditions. In contrast, the complete 2DCWF-CNN framework consistently achieved the highest accuracy across all datasets. This improvement can be attributed to the complementary interaction between 2DCWF-based multi-resolution feature extraction and CNN-based hierarchical feature learning. The ablation results therefore confirm that the performance gain of the proposed method is not due to the CNN classifier alone, but to the integration of Chebyshev wavelet feature enhancement with deep classification.

Table 3

Ablation Analysis of the Proposed 2DCWF-CNN Framework across Benchmark Iris Datasets

Dataset	CNN only Accuracy (%)	2DCWF-HD Accuracy (%)	Conventional descriptors-CNN Accuracy Range (%)	2DCWF-CNN Accuracy (%)
MMU.v2	93.84	95.62	92.45–94.92	96.95
UBIRIS.v2	90.73	93.41	89.15–92.65	94.99
CASIA.v4-Int	96.12	97.86	94.55–96.03	98.97
CASIA.v4-Distance	91.58	93.72	90.72–92.56	94.89

The experimental results demonstrate that the proposed 2DCWF-CNN framework consistently outperformed the conventional feature extraction methods across all benchmark datasets. This performance improvement can be attributed to the complementary integration of Chebyshev wavelet-based spatial-frequency feature extraction and CNN-based hierarchical classification. Unlike LBP, which mainly captures local grey-level texture transitions, and GWF, which is sensitive to scale and orientation selection, the 2DCWF provides an orthogonal and multi-resolution representation of iris texture. This enables the framework to capture both coarse and fine discriminative iris patterns, including radial furrows, crypts, collarette structures, and local intensity variations. As a result, the proposed model achieved stronger recognition performance under both controlled and unconstrained acquisition conditions.

Table 4 presents the comparative performance of four feature extraction techniques -LBP, GWF, LWF, and the proposed 2DCWF across four benchmark iris datasets using FAR, FRR, GAR, and overall accuracy as evaluation metrics. These metrics provide a more comprehensive assessment than accuracy alone because they reflect both the security and usability dimensions of biometric recognition. A lower FAR indicates stronger resistance to false acceptance of impostors, while a lower FRR reflects improved acceptance of genuine users. Similarly, GAR indicates the proportion of genuine users correctly accepted by the system, making it particularly important for assessing operational reliability. For the MMU.v2 dataset, the proposed 2DCWF achieved the best overall performance, with the lowest FAR of 3.18%, the lowest FRR of 3.15%, the highest GAR of 96.85%, and the highest accuracy of 96.95%. This indicates that the 2DCWF provides a more discriminative feature representation than the conventional descriptors under moderate variations in illumination and subject positioning. The improved performance can be attributed to the multi-resolution and orthogonal properties of the Chebyshev wavelet, which allow the method to capture fine iris texture details while reducing redundant feature information. Although GWF and LWF also demonstrated competitive performance, LWF slightly outperformed GWF in GAR and accuracy, suggesting that wavelet-based representations are generally more effective than purely local texture descriptors for iris recognition. In contrast, LBP recorded the weakest performance, with the highest FAR and FRR values of 6.78% and 7.70%, respectively, and an accuracy of 92.45%. This result suggests that LBP is more sensitive to local intensity variations and may be less robust when the iris texture contains illumination changes or minor acquisition inconsistencies.

Table 4

Comparative Results Analysis between 2DCWF wit Others

Database	Method	FAR (%)	FRR (%)	GAR (%)	Accuracy (%)
MMU.v2	LBP	6.78	7.70	92.30	92.45
	GWF	4.05	5.96	94.01	94.31
	LWF	4.20	5.20	94.80	94.92
	2DCWF	3.18	3.15	96.85	96.95
UBIRIS.v2	LBP	8.67	11.05	88.95	89.15
	GWF	8.09	10.16	89.84	89.94
	LWF	6.61	8.35	91.65	92.65
	2DCWF	4.17	5.07	94.93	94.99

(continued)

Database	Method	FAR (%)	FRR (%)	GAR (%)	Accuracy (%)
CASIA.v4 INTERVAL	LBP	4.56	5.67	94.33	94.73
	GWF	4.80	5.85	94.15	94.55
	LWF	3.51	4.79	95.21	96.03
	2DCWF	1.02	1.17	98.83	98.97
CASIA.v4 DISTANCE	LBP	8.93	9.35	90.65	91.15
	GWF	8.22	9.95	90.05	90.72
	LWF	6.15	7.75	92.25	92.56
	2DCWF	3.07	5.83	94.17	94.89

For the UBIRIS.v2 dataset, which contains visible-spectrum and unconstrained iris images affected by noise, reflections, motion blur, eyelid/eyelash occlusion, and illumination variation, the performance gap among the methods became more pronounced. The proposed 2DCWF achieved the best result, with a FAR of 4.17%, FRR of 5.07%, GAR of 94.93%, and accuracy of 94.99%. This confirms the robustness of the 2DCWF in extracting stable spatial-frequency features from degraded iris images. The relatively strong performance of LWF, with an accuracy of 92.65%, further supports the usefulness of wavelet-based feature extraction in challenging biometric scenarios. However, GWF and LBP produced lower accuracies of 89.94% and 89.15%, respectively, indicating that these techniques are more vulnerable to unconstrained image conditions. The weaker performance of GWF may be linked to its sensitivity to scale, orientation, and parameter selection, while LBP is affected by local noise and non-uniform illumination. Overall, the UBIRIS.v2 results demonstrate that the proposed 2DCWF is better suited for real-world iris recognition conditions where the iris texture may be partially degraded, occluded, or captured under non-ideal illumination.

Figure 8 provides a comparative visual summary of the recognition accuracy achieved by LBP, GWF, LWF, and the proposed 2DCWF across the four benchmark iris datasets. The figure shows that the proposed 2DCWF consistently achieved the highest accuracy across all datasets, demonstrating the stability and generalisability of the method under different acquisition conditions. This consistency is important because a robust iris recognition framework should not only perform well on controlled datasets but should also maintain reliable accuracy when tested on unconstrained and degraded iris images. The best performance was observed on CASIA.v4-Interval, where 2DCWF achieved an accuracy of 98.97%. This result is expected because CASIA.v4-Interval consists of relatively high-quality near-infrared iris images captured under more controlled conditions. Under such conditions, iris texture is better preserved, segmentation is more reliable, and the discriminative advantage of the 2DCWF becomes more pronounced. The high accuracy suggests that the Chebyshev wavelet representation effectively captures both fine and coarse iris texture patterns when the input image quality is favourable. On MMU.v2, the proposed method also recorded good performance with an accuracy of 96.95%, confirming its effectiveness under moderate variations in illumination and subject positioning. The ability of 2DCWF to maintain high accuracy on this dataset indicates that its multi-resolution decomposition and orthogonal basis representation provide stable feature encoding even in the presence of minor acquisition inconsistencies. This supports the suitability of the method for biometric systems operating under semi-controlled conditions.

Figure 8

Accuracy Comparison of Different Techniques across Datasets

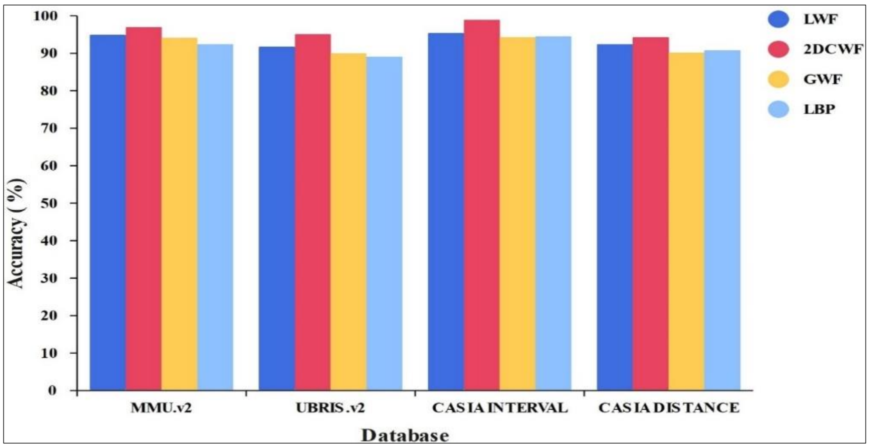

The performance difference becomes meaningful on UBIRIS.v2 and CASIA.v4-Distance, which are more challenging datasets. UBIRIS.v2 contains visible-spectrum iris images affected by noise, reflections, non-uniform illumination, motion blur, and occlusions, while CASIA.v4-Distance includes images captured at longer distances and with greater variation in gaze direction and iris scale. Despite these challenges, 2DCWF achieved the highest accuracies of 94.99% and 94.89%, respectively. These results indicate that the proposed method is not merely optimised for controlled datasets but can preserve discriminative iris features under degraded and unconstrained acquisition conditions.

In comparison, LWF generally ranked second across the datasets, showing that wavelet-based feature extraction remains effective for iris recognition. However, its accuracy remained consistently lower than that of 2DCWF, suggesting that the Chebyshev wavelet provides a more discriminative spatial-frequency representation. GWF and LBP showed comparatively weaker performance, especially on UBIRIS.v2 and CASIA.v4-Distance. This decline may be attributed to the sensitivity of GWF to scale, orientation, and parameter selection, while LBP is more vulnerable to local noise, illumination variation, and degraded texture contrast.

Figure 9 illustrates the comparative performance of four feature extraction techniques based on their FRR as a function of FAR. It critically assesses the security-usability trade-off, a cornerstone metric in biometric system evaluation. Among all techniques, CWF consistently yields the lowest FRR across the entire FAR spectrum (0% to 9%), indicating superior discriminatory power. It also achieves an impressively low FRR of 1.17%, underscoring its robustness in rejecting impostors while minimizing false rejections of genuine users. CWF maintains FRR values below 6% even as FAR increases, outperforming the other methods by a notable margin.

Figure 9

ROC Curves of Different Feature Extraction Techniques

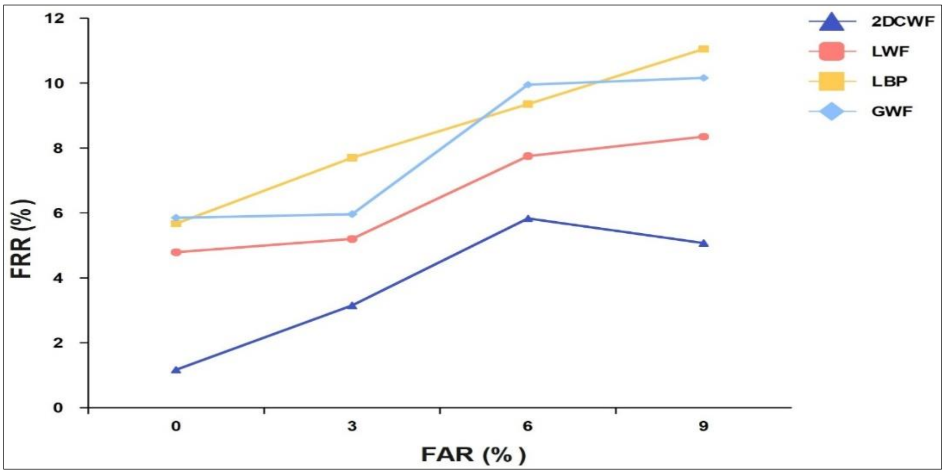

LWF performs moderately, gradually increasing FRR from approximately 5% to 8% as FAR rises. Even though it is more stable than LBP and GWF, LWF lags behind 2DCWF in minimizing rejection errors, suggesting that it may be better suited for environments where computational efficiency is prioritized over absolute accuracy. It has been observed that the overall trend reveals that CWF exhibits the most favourable FAR–FRR trade-off curve due to its capacity for capturing multi-scale frequency features while maintaining robustness to occlusions and partial iris visibility. This makes it a compelling choice for next-generation iris recognition systems, especially in security-critical applications requiring both high precision and tolerance to degraded input quality.

The average computational time required by the proposed 2DCWF-CNN framework for feature extraction and recognition across the four benchmark iris datasets are presented Table 5. The runtime analysis was included to complement the accuracy, FAR, FRR, and GAR results since practical biometric systems must achieve not only high recognition performance but also computational feasibility. Recent iris recognition studies emphasise that robustness and efficiency are both important for real-world biometric deployment, particularly when deep learning models are used for segmentation, feature extraction, and recognition under unconstrained acquisition conditions. The results show that feature extraction time ranged from 79 ms to 112 ms, while recognition time ranged from 29 ms to 38 ms. CASIA.v4-Interval recorded the lowest processing time, with 79 ms for feature extraction and 29 ms for recognition. This can be attributed to the relatively controlled near-infrared acquisition conditions of CASIA.v4-Interval, where iris texture is clearer, segmentation is more stable, and fewer degraded regions affect the feature extraction process. In contrast, UBIRIS.v2 recorded the highest feature extraction time of 112 ms and recognition time of 38 ms. This is expected because UBIRIS.v2 contains visible-spectrum and unconstrained iris images affected by illumination variation, reflections, occlusions, and image noise, which typically increase the computational burden during robust feature extraction and classification.

Table 5

Average Feature Extraction and Recognition Time of the Proposed 2dcwf-Cnn Framework across Benchmark Iris Datasets

Dataset	Feature Extraction Time (ms)	Feature Recognition Time (ms)
UBIRIS.v2	112	38
MMU.v2	84	31
CASIA.v4. Interval	79	29
CASIA.v4.Distance	106	36

The runtime pattern also shows that CASIA.v4-Distance required higher processing time than CASIA.v4-Interval, with 106 ms feature extraction time and 36 ms recognition time. This reflects the additional complexity introduced by distance-based image acquisition, where iris regions may appear smaller, less sharply defined, and more affected by off-angle positioning. These conditions can increase the cost of localised spatial-frequency analysis because the model must preserve discriminative iris texture despite scale variation and partial degradation. Recent work on adaptive iris feature extraction similarly highlights that reduced resolution, blur, and less-constrained acquisition conditions directly affect the reliability and complexity of feature extraction. The relatively low recognition time across all datasets indicates that, once the 2DCWF feature representation has been extracted, the CNN classifier performs identity recognition efficiently. This is important because the main computational cost of the proposed framework lies in the wavelet-based feature extraction stage rather than the final classification stage. The use of 2DCWF is therefore justified because it introduces only moderate processing overhead while improving recognition performance across controlled and unconstrained datasets. Therefor, the runtime results demonstrate that the proposed 2DCWF-CNN framework is computationally practical for biometric authentication. The average feature extraction time of approximately 95.25 ms and average recognition time of approximately 33.50 ms indicate that the method can process iris samples within a reasonable time while maintaining strong recognition accuracy.

Performance Comparison

To evaluate the effectiveness of the proposed 2DCWF-CNN framework, its performance was compared with recent iris recognition approaches which are presented in Table 6. Earlier methods such as the V-Net-based architecture with colour-space segmentation reported 95.6% accuracy, while the integration of multi-level Otsu thresholding with the Daugman algorithm improved recognition accuracy from 94.23% to 96.60%. Similarly, fuzzy logic combined with enhanced Morlet wavelet transform achieved 85.43% accuracy, indicating the relevance of wavelet-based feature extraction. More recent studies have shown improved performance through advanced learning frameworks; for example, TT-GAN improved recognition accuracy from 59.72% to 93.42%, while Histogram Cut Selection with Genetic Algorithm optimisation achieved 97.8% testing accuracy by improving feature selection and classification robustness.

Table 6

Performance Comparison of the Proposed Approach with Related Approaches

Author/Year	Approach	Accuracy
(Banerjee et al., 2022)	V-Net-based architecture and color-space segmentation technique to refine iris boundaries.	Achieved 95.6% accuracy
(Virtusio et al., 2022)	Multi-level Otsu thresholding and the Daugman algorithm on a Raspberry Pi platform.	Improved recognition accuracy from 94.23% to 96.60%
(Regencia et al., 2023)	Integration of fuzzy logic and enhanced Morlet wavelet transform for feature extraction. was achieved.	The approach achieved 85.43% accuracy
(Chen et al., 2024)	Two-Stage and Two-Discriminator Generative Adversarial Network (TT-GAN), and a Pixel–Channel (PC) dual SN-PatchGAN discriminators.	The recognition accuracy is improved form 59.72% - 93.42%
(Sharma et al., 2025)	Histogram Cut Selection with Genetic Algorithm-optimised classifier	98.7% training accuracy; 97.8% testing accuracy; 97.7% validation accuracy
(Rahman et al., 2025)	Customized CNN/VGG16/VGG19/ResNet50 features + ML classifiers	93.40% accuracy
(Louriga et al., 2026)	MEEMD + VGG16 + ResNet-152 + LBP + PCA	98% IITD; 97% CASIA; 97.30% UBIRIS.v2
Present Study	Two-Dimensional Chebyshev Wavelet Filter integrated with CNN classifier	**Best accuracy at 98.97%**

Moreover, Deep learning-based approaches have also shown good results, achieving 93.40% accuracy using customised CNN and transfer-learning features (Rahman et al., 2025). Also, Louriga et al. (2026) reporting 98% on IITD, 97% on CASIA, and 97.30% on UBIRIS.v2 using MEEMD, dual CNNs, LBP, and PCA-based feature fusion. In comparison, the present 2DCWF-CNN framework achieved a best recognition accuracy of 98.97%. The Two-Dimensional Chebyshev Wavelet Filter-based multi-resolution spatial-frequency feature extraction with CNN classification provides a competitive and robust solution for iris recognition across controlled and unconstrained datasets. This result suggests that the proposed method retains the interpretability and texture sensitivity of wavelet-based analysis while benefiting from the hierarchical discriminative learning capacity of CNNs.

CONCLUSION AND FUTURE WORK

This study introduced a novel iris recognition framework that integrates a Two-Dimensional Chebyshev Wavelet Filter (2DCWF) with a CNN for enhanced feature extraction and classification. Through rigorous experimentation on four benchmark iris datasets, the proposed model consistently outperformed conventional techniques such as LBP, GWF, and LWF across multiple performance metrics, including FAR, FRR, GAR, and accuracy. Notably, the 2DCWF-based method achieved the highest recognition accuracy of 98.83% on CASIA-Interval and maintained robust performance under unconstrained and noisy conditions, such as in the UBIRIS.v2 and CASIA-Distance datasets. Its capacity to capture multi-scale texture details with compact support, orthogonality, and localized frequency resolution proves highly effective for biometric scenarios plagued by occlusions, illumination variations, and partial iris visibility. Although the proposed 2DCWF-CNN framework demonstrated strong recognition performance across CASIA.v4, UBIRIS.v2, and MMU datasets, some limitations remain. The study was evaluated using benchmark datasets; therefore, further validation using larger, more diverse, and operationally acquired iris datasets is necessary to assess generalisability in real-world biometric environments. Poor segmentation may still affect the quality of extracted iris features, especially if the threshold value is below 12.5%, then the system can not authenticate an individual. Future research will therefore focus on real-time implementation and fusion of 2DCWF with attention-based deep learning models to further improve robustness under unconstrained iris acquisition conditions.

ACKNOWLEDGMENT

This study did not receive any specific grant from funding agencies in the public, commercial, or not-for-profit sectors.

REFERENCES

Almolhis, N. A. (2024). *An biometric model for iris images segmentation and deep learning classification*. 2024 IEEE 11th International Conference on Data Science and Advanced Analytics (DSAA) (pp. 1-6). IEEE. https://doi.org/10.1109/DSAA61799.2024.10722825AlRifaee,

Almanasra, S., Hnaif, A., Althunibat, A., Abdallah, M., & Alrawashdeh, T. (2024). Adaptive segmentation for unconstrained iris recognition. *Computers, Materials & Continua, 78*(2), 1591–1608. https://doi.org/10.32604/cmc.2023.043520

Banerjee, A., Ghosh, C., & Mandal, S. N. (2022). Analysis of v-net architecture for iris segmentation in unconstrained scenarios. *SN Computer Science, 3*(3), 208. https://doi.org/10.1007/s42979-022-01113-0

Bonyani, M., Ghanbari, M., & Rad, A. (2022). Different gaze direction (DGNet) collaborative learning for iris segmentation. *SSRN Electronic Journal*. https://doi.org/10.2139/ssrn.4237124

Boutros, F., Kaehm, O., Fang, M., Kirchbuchner, F., Damer, N., & Kuijper, A. (2022). *Low-resolution iris recognition via knowledge transfer*. Proceedings of the 2022 International Conference of the Biometrics Special Interest Group (BIOSIG). https://doi.org/10.1109/BIOSIG 55365.2022.9896959

Chen, Y., Wu, C., & Wang, Y. (2020). T-Center: A novel feature extraction approach towards large-scale iris recognition. *IEEE Access*, *8*, 32365-32375. https://doi.org/10.1109/ACCESS. 2020.2973433

Chen, Y., Xu, L., Chen, H., Zeng, Y., Guo, S., Deng, J., & Heidari, A. A. (2024). Two-stage and two-discriminator generative adversarial network for the inpainting of irregularly incomplete iris images. *Displays*, *82*, 102626. https://doi.org/10.1016/j.displa.2023.102626

Czajka, A., Moreira, D., Bowyer, K. W., & Flynn, P. J. (2019). *Domain-specific human-inspired binarized statistical image features for iris recognition*. Proceedings of the IEEE Winter Conference on Applications of Computer Vision (WACV), 959–967. https://doi.org/10.1109/ WACV.2019.00107

Dahan, N. A., & Jaha, E. S. (2025). IRIS-QResNet: A quantum-inspired deep model for efficient iris biometric identification and authentication. *Sensors*, *26*(1), 121. https://doi.org/10.3390/ s26010121

Danlami, M., Jamel, S., Ramli, S. N., & Azahari, S. R. M. (2020). C*omparing the Legendre wavelet filter and the Gabor wavelet filter for feature extraction in an iris recognition system*. Proceedings of the 2020 IEEE 6th International Conference on Optimization and Applications (ICOA) (pp. 1–6). IEEE. https://doi.org/10.1109/ICOA49421.2020.9094465

Daugman, J. (2004). How iris recognition works. *IEEE Transactions on Circuits and Systems for Video Technology*, *14*(1), 21-30. https://doi.org/10.1109/TCSVT.2003.818350

Divya, C. D., & Rajendra, A. B. (2022). Performance analysis of feature extraction approach: Local binary pattern and principal component analysis for iris recognition system. *International Journal of Electrical and Electronics Research*, *10*(2), 57-61. https://doi.org/10.37391/IJEER.100201

Farmanullah, J. (2026). Robust iris segmentation with deep CNNs for detecting fully or nearly closed eyes in non-ideal biometric systems. *Computers*, *15*(4), 253. https://doi.org/10.3390/computers15040253

Farouk, R. H., Mohsen, H., & Abd El-Latif, Y. M. (2022). *Iris recognition system techniques: A literature survey and comparative study*. Proceedings of the 5th International Conference on Computing and Informatics (ICCI) (pp. 194–199). IEEE. https://doi.org/10.1109/ICCI54321.2022.9756079

Fathi, A., & Mohamadi, M. (2019). Metric-learning-based high-discriminative local features extraction for iris recognition. *Pattern Analysis and Applications*, *22*(4), 1427-1438. https://doi.org/10.1007/s10044-018-0713-4

Guariglia, E., & Guido, R. C. (2022). Chebyshev wavelet analysis. *Journal of Function Spaces*, *2022*(12), 1-17. https://doi.org/10.1155/2022/5542054

Guo, Y., Wang, Q., Huang, H., Zheng, X., & He, Z. (2019). *Adversarial iris super resolution*. 2019 International Conference on Biometrics (ICB) (pp. 1–8). IEEE. https://doi.org/10.1109/ICB45273.2019.8987243

Guo, S., Chen, Y., Xu, L., Deng, J., Chen, H., & Heidari, A. A. (2025). Multiscale attention feature deep fusion network for iris region localization and segmentation from dual-spectral iris image. *Applied Soft Computing*, *179,* 113334. https://doi.org/10.1016/j.asoc.2025.113334

He, S., & Li, X. (2024). EnhanceDeepIris model for iris recognition applications. *IEEE Access*, *12*, 66809-66821. https://doi.org/10.1109/ACCESS.2024.3388169.

Huo, G., Guo, H., Zhang, Y., Zhang, Q., Li, W., & Li, B. (2019). An effective feature descriptor with gabor filter and uniform local binary pattern transcoding for iris recognition. *Pattern Recognition and Image Analysis*, *29*(4), 688-694. https://doi.org/10.1134/S1054661819040059

Hussein, H. I., Abduallah, W. M., & Omer, H. K. (2026). Iris recognition based deep learning: A survey. *Dasinya Journal for Engineering and Informatics, 2*(1). https://doi.org/10.65542/djei.v2i1.17

Ibrahim, Y. I., & Sultan, E. A.-J. (2023). Iris recognition based on 2D Gabor filter. *International Journal of Electrical and Computer Engineering (IJECE)*, *13*(1), 325–334. https://doi.org/10.11591/ijece.v13i1.pp325-334

Jagadeesh, N., & Patil, C. M. (2018). *Conceptual view of the iris recognition systems in the biometric world using image processing techniques*. Proceedings of the International Conference on Computing Methodologies and Communication, ICCMC 2017, 2018-Janua(Iccmc), 1018-1022. https://doi.org/10.1109/ICCMC.2017.8282623

Jalal, R. W., & Ghanim, M. F. (2022). *Segmentation techniques in iris recognition system*. Proceedings of the 2022 IEEE Integrated STEM Education Conference (ISEC) (pp. 444–449). IEEE. https://doi.org/10.1109/ISEC54952.2022.10025158

Jalilian, E., Wimmer, G., Uhl, A., & Karakaya, M. (2022, May). *Deep learning based off-angle iris recognition*. ICASSP 2022-2022 IEEE International Conference on Acoustics, Speech and Signal Processing (ICASSP) (pp. 4048-4052). IEEE. https://doi.org/10.1109/ICASSP43922.2022.9746090.

Jamaludin, S., Zainal, N., & Zaki, W. M. D. W. (2021). Deblurring of noisy iris images in iris recognition. *Bulletin of Electrical Engineering and Informatics, 10*(1), 156–159. https://doi.org/10.11591/eei.v10i1.2467

Kawakami, S., Kawai, H., Ito, K., Aoki, T., Yasumura, Y., Fujio, M., Kaga, Y., & Takahashi, K. (2022). *A simple and accurate CNN for iris recognition*. Proceedings of the 2022 Asia-Pacific Signal and Information Processing Association Annual Summit and Conference (APSIPA ASC) (pp. 1566–1571). IEEE. https://doi.org/10.23919/APSIPAASC55919.2022.9980056

Kumawat, A., & Panda, S. (2023). Noisy iris smoothing and segmentation scheme based on improved Wildes method. *Multidimens Syst Signal Process*, *34*(1), 47-79. https://doi.org/10.1007/s11045-022-00852-w

Louriga, Z. E., Jabri, I., El Ouaazizi, A., & Affar, A. E. (2026). A hybrid multi-domain feature fusion model integrating MEEMD and dual CNN for iris recognition. *Machine Learning and Knowledge Extraction*, *8*(4), 111. https://doi.org/10.3390/make8040111

Luo, Y., Zhao, X., Shen, H., Fu, C., & Jiang, H. (2025). A novel deep learning network for iris recognition using non-global interactive channel attention and lightweight spatial attention. *Signal, Image and Video Processing, 19*(11), 950. https://doi.org/10.1007/s11760-025-04561-2

Malgheet, J. R., Manshor, N. B., Affendey, L. S., & Lopez Gutierrez, R. M. (2021). Iris recognition development techniques: A comprehensive review. *Complexity*, *2021*(1). https://doi.org/10.1155/2021/6641247

Miyazawa, K., Ito, K., Aoki, T., Kobayashi, K., & Nakajima, H. (2008). An effective approach for iris recognition using phase-based image matching. *IEEE Transactions on Pattern Analysis and Machine Intelligence, 30*(10), 1741–1756. https://doi.org/10.1109/TPAMI.2007.70833

Mukherjee, A., Islam, M. Z., Mamun-Al-Imran, G. M., & Ali, L. E. (2021). *Iris recognition using wavelet features and various distance based classification*. Proceedings of International Conference on Electronics, Communications and Information Technology, ICECIT 2021(September), 1-4. https://doi.org/10.1109/ICECIT54077.2021.9641118

Nguyen, K., Fookes, C., Sridharan, S., & Ross, A. (2023). Complex-valued iris recognition network. *IEEE Transactions on Pattern Analysis and Machine Intelligence*, *45*(1), 182-196. https://doi.org/10.1109/TPAMI.2022.3152857

Nguyen, K., Proença, H., & Alonso-Fernandez, F. (2024). Deep learning for iris recognition: A survey. *ACM Computing Surveys, 56*(9), 1-35. https://doi.org/10.1145/3651306

Nithya, A. A., & Lakshmi, C. (2019). Enhancing iris recognition framework using feature selection and BPNN. *Cluster Computing*, *22*(Suppl 5), 12363-12372. https://doi.org/10.1007/s10586-017-1619-4

Nsaif, A. K., Ali, S. H. M., Nseaf, A. K., Jassim, K. N., Al-Qaraghuli, A., & Sulaiman, R. (2022). Robust and swift iris recognition at distance based on novel pupil segmentation. *Journal of King Saud University-Computer and Information Sciences*, *34*(10), 9184-9206. https://doi.org/10.1016/j.jksuci.2022.09.002

Rahman, M. A., Ali, L. E., Mistry, S. K., Mukherjee, A., & Islam, M. Z. (2025). Distant iris recognition through machine learning models with deep features transfer for human identification. *Journal of Innovative Image Processing, 7*(3), 840-860. https://doi.org/10.36548/jiip.2025.3.014

Rathgeb, C., Wagner, J., & Busch, C. (2019). SIFT-based iris recognition revisited: Prerequisites, advantages and improvements. *Pattern Analysis and Applications*, *22*(3), 889-906. https://doi.org/10.1007/s10044-018-0719-y

Rathnayake, R., Madhushan, N., Jeeva, A., Darshani, D., Subasinghe, A., Silva, B. N., Wijesingha, L., & Wijenayake, U. (2023). Current trends in human pupil localization: A review. *IEEE Access*, *11*(September), 115836-115853. https://doi.org/10.1109/ACCESS.2023.3325293

Regencia, G. A., Gaba, C. B., & Linsangan, N. (2023). *Morlet wavelet-based feature extraction algorithm with fuzzy logic for an iris recognition system for non-ideal images*. Proceedings of the 2023 IEEE 15th International Conference on Humanoid, Nanotechnology, Information Technology, Communication and Control, Environment, and Management (HNICEM) (pp. 1–6). IEEE. https://doi.org/10.1109/HNICEM60674.2023.10589181

Rhif, M., Abbes, A. B., Farah, I. R., Martínez, B., & Sang, Y. (2019). Wavelet transform application for/in non-stationary time-series analysis: A review. *Applied Sciences*, *9*(7), 1-22. https://doi.org/10.3390/app9071345

Şerifi, M., & Şerifi, Ü. (2025). Dual CNN and texture-based face-iris multimodal biometric system via decision-level fusion. *Signal, Image and Video Processing*, *19*(4), 292. https://doi.org/10.1007/s11760-025-03873-7

Sharma, A., Kumar, D., & Gupta, G. (2025). Enhanced iris recognition with histogram cut selection and genetic algorithms for robust classification. *Procedia Computer Science*, *258*, 2846-2859. https://doi.org/10.1016/j.procs.2025.04.545

Shoji, Y., Ogino, Y., Toizumi, T., & Ito, A. (2024). *Adaptive deep iris feature extractor at arbitrary resolutions.* Proceedings of the 2024 IEEE International Joint Conference on Biometrics (IJCB) (pp. 1–10). IEEE. https://doi.org/10.1109/IJCB62174.2024.10744472

Sun, J., Zhao, S., Yu, Y., Wang, X., & Zhou, L. (2022). Iris recognition based on local circular Gabor filters and multi-scale convolution feature fusion network. *Multimedia Tools and Applications*, *81*(23), 33051-33065. https://doi.org/10.1007/s11042-022-13098-2

Taha, M. A., & Ahmed, H. M. (2021). *Iris features extraction and recognition based on the local binary pattern technique.* Proceedings of the 2021 International Conference on Advanced Computer Applications (ACA) (pp. 16–21). IEEE. https://doi.org/10.1109/ACA52198.2021.9626827

Toizumi, T., Takahashi, K., & Tsukada, M. (2023). *Segmentation-free direct iris localization networks*. Proceedings of the IEEE/CVF Winter Conference on Applications of Computer Vision (WACV), 991–1000. https://doi.org/10.1109/WACV56688.2023.00105

Virtusio, D. T. U., Tapaganao, F. J. D., & Maramba, R. G. (2022, July). *Enhanced iris recognition system using Daugman algorithm and multi-level Otsu's thresholding*. 2022 International Conference on Electrical, Computer and Energy Technologies (ICECET) (pp. 1-6). IEEE. doi: 10.1109/ICECET55527.2022.9873032.

Wei, J., Huang, H., Wang, Y., He, R., & Sun, Z. (2022). Towards more discriminative and robust iris recognition by learning uncertain factors. *IEEE Transactions on Information Forensics and Security*, *17*, 865–879. https://doi.org/10.1109/TIFS.2022.3154240

Zambrano, J. E., Benalcazar, D. P., Perez, C. A., & Bowyer, K. W. (2022). Iris recognition using low-level CNN layers without training and single matching. *IEEE Access*, *10*, 41276-41286. https://doi.org/10.1109/ACCESS.2022.3166910

Zhao, Q., Jiang, J., Lei, Z., & Yi, J. (2021). Detection method of eyes opening and closing ratio for driver's fatigue monitoring. *IET Intelligent Transport Systems*, *15*(1), 31-42. https://doi.org/10.1049/itr2.12002